Effects of composition and crystallographic ordering on the ferromagnetic transition in Ni-Co-Mn-In magnetic shape memory alloys

D. Salas[a], O. Eliseeva[a], Y. Wang[a], T. Duong[a], Y.I. Chumlyakov[b], Y. Ren[c], R. Arroyave[a], I. Karaman[a]*

[a] Department of Materials Science and Engineering, Texas A&M University, College Station, TX, 77843, USA

[b] Siberian Physical and Technical Institute, Tomsk State University, 634050, Tomsk, Russia

[c] X-ray Science Division, Advanced Photon Source, Argonne National Laboratory, Lemont, IL, 60439, USA

Abstract

In the present study, the effects of composition and the level of crystallographic ordering were studied in $Ni_{45}Co_5Mn_{50-X}In_X$ magnetic shape memory alloys with X = 13.55, 13.71 and 13.92, in order to reveal the relationship between the Curie temperature (T_C) of the austenite phase and the degree of $L2_1$ ordering. Various samples were prepared using secondary heat treatments at different temperatures below the order-disorder transition temperature and for different durations, after solution heat treatment, in order to control the degree of ordering. T_Cs were determined using calorimetric and magnetometry measurements. The relationship between the T_C and the degree of order was used to predict the evolution of the order during selected heat treatments. It was shown that the T_C of austenite exhibits a monotonous non-linear dependence on the fraction of the $L2_1$ phase. This relationship was corroborated via ab initio numerical calculations within a mean field approximation. Dependence of the crystallographic order parameter on temperature and duration of secondary heat treatments showed that ordering kinetics is fast, the total degree of order depends only on the annealing temperature and cooling rate for long enough treatments, and maximum achievable degree of order is limited by the low thermal energy available for atomic diffusion at low temperatures. Finally, small changes in composition were observed to have a significant impact on martensitic transformation temperatures, and a significant but smaller effect on the ferromagnetic transition in these systems.

* Corresponding author. E-mail address: ikaraman@tamu.edu (I. Karaman).

Keywords
Magnetic shape memory alloys, Degree of order, Curie temperature, Martensitic transformation, Ferromagnetic transition

1. Introduction

Ni-Mn-based MetaMagnetic Shape Memory Alloys (MMSMAs) have received much attention due to their unique properties, such as conventional shape memory effect[[1], [2], [3], [4], [5]], magnetic field-induced martensitic transformation (MT) [6,7], giant magnetocaloric effect [[8], [9], [10], [11], [12]] and large magnetoresistance [13]. Many of these properties emerge from the MT between a ferromagnetic cubic austenite and the superparamagnetic or anti-ferromagnetic, non-modulated 2 M or modulated (5 M, 7 M) tetragonal martensites [14,15]. In order words, MMSMAs demonstrate a magneto-structural transition coupling a ferroelastic and a magnetic transition, in which the magnetic state of the system changes from strongly ferromagnetic to anti-ferromagnetic/super-paramagnetic state upon cooling.

The degree of magnetic ordering (characterized by the Curie temperature of the austenite phase, T_C) has been shown to play a significant role on the MT temperatures of MMSMAs [[16], [17], [18], [19]]. More specifically, in NiCoMnIn MMSMAs, the increase (decrease) of the magnetic ordering of austenite (characterized by T_C) decreases (increases) the total entropy change at the MT [[20], [21], [22]]. This effect results in an inversely proportional relationship between the MT temperatures and the difference between T_C and M_S, where M_S is the martensite start temperature upon cooling. Consequently, MT temperatures can be tuned by tuning magnetic ordering in MMSMAs, allowing for the modification of martensitic transformation characteristics such as transformation hysteresis, transformation range, and degree of transformation suppression [19,23], or for complete suppression of the MT giving rise to the glass transition behavior with potentially unique properties [19,[24], [25], [26], [27], [28], [29]]. Therefore, the present work is focused on investigating one of the ways that can potentially be used to tailor the magnetic ordering (T_C) of austenite, i.e. through the control of the degree of crystallographic order. The different degrees of order can be achieved through simple secondary heat treatments in some of the MMSMAs [19,30], including NiCoMnIn and NiCoMnGa systems. Therefore, in the present work we investigate the role of different degrees of crystallographic ordering in austenite on T_C, where the crystallographic order is controlled via simple heat treatments.

It should be noted that the origin of the different magnetic behaviors in the austenite and martensite phases in MMSMAs is generally the Ruderman-Kittel-Kasuya-Yosida (RKKY)-exchange interaction, which implies an oscillatory behavior of the magnetic exchange constants between pairs of Mn atoms, depending on their interatomic distance. Ab-initio calculations performed by Buchelnikov et al. [31] suggested that the magnetism of austenitic and martensitic phases are determined by the average Mn-Mn bond length. The magnetic moments of nearest-neighbor Ni-Mn atoms (with Ni and Mn atoms on their regular sublattice sites) interact ferromagnetically. However, the interaction between Mn-Mn pairs is predominantly either ferromagnetic or antiferromagnetic depending on the distance between Mn atoms. As a consequence of the MT in MMSMAs, the average distance between Mn-Mn pairs changes upon transformation, resulting in a qualitative change in the nature of the magnetic interactions between Mn-Mn pairs. While the austenite is normally ferromagnetic within the martensitic transformation temperature range, Mn positions in the tetragonal martensite result in a competition of ferromagnetic-antiferromagnetic interactions leading to a superparamagnetic behavior.

In the present MMSMA, the austenite can exist in two different cubic states, B2 and $L2_1$, with different degree of ordering (η_{L21}). The Order-DisOrder (ODO) transition between B2 and $L2_1$ phases requires (short-range) atomic diffusion and its critical temperature depends on composition [32]. Different researchers [16,18,33] have recently reported the effects of η_{L21} on T_C and MT temperatures in MMSMAs. Generally, the formation of an ordered $L2_1$ phase increases T_C and may increase [16] or decrease, as in the present NiCoMnIn system [19], the MT temperatures, depending on whether the martensite or austenite possesses higher magnetic ordering, respectively. It is normally much easier to determine T_C than to evaluate the degree of order in a material. Therefore, in some cases, T_C can be used to evaluate the ordering transition or the degree of order, like Neibecker et al. did in Ni-Mn-Al alloys [34].

Recently, Bruno et al. [28] demonstrated that the MT temperatures could present a minimum as a function of heat treatment time when annealing below the ODO transition temperature in NiCoMnIn MMSMAs. M_S was observed to decrease for short heat treatments while it increased progressively as the heat treatments were carried out for longer times. It has been proposed that this non-monotonic evolution should be caused by different thermally-activated processes occurring during the heat treatment, which affect the material microstructure as well as the phase stability. Bruno et al. results were obtained in a $Ni_{45}Co_5Mn_{36.6}In_{13.4}$ alloy. This composition and nearby $Ni_{45}Co_5Mn_{50-X}In_X$ compositions are of special interest since the MT properties have been shown to be highly sensitive to compositional and microstructural changes for $X = 13.3–13.7$ [15].

Therefore, the present work investigates the dependence of the T_C of the austenite phase and the relationship between the T_C and crystallographic ordering as well as the magnetic properties on secondary heat treatments below the ODO transition temperature for different NiCoMnIn alloys. Then, T_C is used to probe the evolution of η_{L21} and to establish a relationship with the evolution of MT temperatures. The main motivation of the present work is to test the hypothesis that by correlating η_{L21} to changes in T_C, it should be possible to correlate heat treatment schedules with η_{L21}, and thus, shed light on the mechanisms responsible for the high sensitivity of the MT to secondary heat treatments in MMSMAs.

2. Experimental methods

2.1. Material synthesis and annealing parameters

Three polycrystalline NiMnCoIn alloys, with the measured compositions given in Table 1 (called as In13.55, In13.71 and In13.92 in what follows, based on their In content), were fabricated using vacuum induction melting of high purity elements. The samples with the sizes of $40 \times 5 \times 1$ mm^3 were cut using wire electrical discharge machining (EDM), and sealed in quartz tubes in a protective low-pressure Ar atmosphere. A Solution Heat Treatment (SHT)/homogenization was performed at 1173 K for 24 h. The material was then water-quenched in order to retain a significant degree of disorder (presumably B2 phase [19,28]). Then, smaller specimens were cut using wire EDM from these SHT samples, and sealed in quartz tubes under the argon atmosphere for Secondary Heat Treatments (SecHT). These treatments were performed at different temperatures, between 573 K and 873 K, below the order-disorder transition temperature for the durations from 0.25 h to 240 h. Then, the samples were water-quenched to freeze the degree of $L2_1$ order achieved at that temperature. Selected SecHTs created a large variety of microstructures, with different degrees of $L2_1$ crystallographic ordering, and a variety of domain sizes and morphologies. Another set of samples were Furnace Cooled (FC) from 1173 K to 300 K inside the quartz ampoule at rates of 0.55 K/min. SHT, FC and SecHT samples of each composition were investigated using Scanning Electron Microscopy (SEM), and their compositions were measured using a Cameca SXFive Electron Microprobe Analyzer (EPMA) using wavelength dispersive spectroscopy (WDS), operated at 15 KeV and 20 mA. No precipitation was detected. The transformation temperatures of the MT of the present compositions were observed to decrease with increasing In-content. Fig. 1 presents a comparison between the M_S temperature obtained for SHT samples of polycrystalline $Ni_{45}Co_5Mn_{50\text{-}X}In_X$ MMSMAs, including the present compositions (using measured In-content) and data available in the literature [15,35]. This figure shows that M_S presents a strong Mn/In content dependence from In = 13 to 14 at.% and that present work compositions and previous data follow the same trend in In-content dependence. Given the strong composition-dependence of M_S, the good agreement in the data corroborates the WDS measurements.

2.2. Experimental protocols

Calorimetric measurements were performed for the selected compositions and thermal procedures using a TA Instruments DSC Q2000. The cooling/heating rate was 10 K min^{-1} over a temperature range of 170 K–420 K, spanning the magnetic transition and, in some cases, the MT. Note that atomic diffusion is not expected to occur within this temperature range, and thus, the degree of order is not expected to be affected in a noticeable manner during these measurements. An example of the typical calorimetric response close to the ferromagnetic transition is shown in Fig. 2a. The magnetic transition produces a change in the calorimetric response of the material because of the change in heat capacity [36]. Based on the differential scanning calorimetry (DSC) responses, Curie temperature is estimated averaging the peak temperatures of the first derivative of the calorimetric response for the cooling and heating curves of two consecutive thermocycles, as shown in Fig. 2b. Note that observed small hysteresis, about 0.5 K, in Fig. 2b is an artifact of the calorimetric response as the cooling/heating rate is moderate (10 K min^{-1}). Such source of error was corrected by averaging between T_Cs obtained using cooling and heating curves. To corroborate the obtained T_C values, a Quantum Design MPMS SQUID VSM magnetometer was used to measure the temperature dependence of the DC magnetization under the constant applied magnetic field of 0.05 T. Fig. 2c shows how similar T_C values were detected from the temperature derivative of the DC magnetization responses. These magnetic measurements were performed during cooling–heating cycles between 400 K and 10 K at a rate of 5 K min^{-1}. While it was observed that the calorimetric and magnetic measurements showed almost perfect match, T_C in some samples was higher than the temperature limit of the SQUID magnetometer. Thus, in this work, in order to carry out consistent comparisons across all the heat treatment conditions considered, only the T_Cs determined from the DSC experiments are reported.

In order to corroborate the correlation between T_C and $L2_1$ degree of order, transmission X-Ray Diffraction experiments were conducted at the Advance Photon Source of Argonne National Laboratory (Lemont) using the high-energy synchrotron radiation with wavelength 0.1173 Å. For such experiments, single crystal ingots of nominal composition $Ni_{45}Co_5Mn_{36.6}In_{13.4}$ at.% (In13.4) were grown via the Bridgman method under He environment and thermally processed following the same SHT protocol used for the polycrystalline alloys. Polar diffraction spectra for different SHT In13.4 samples were obtained at 423 K (in austenite). In order to mimic the evolution of the degree of order during conventional heat treatments, SHT samples were heated at 25 K/min from room temperature to different temperatures, i.e. 680 K, 745 K and 790 K, below the ODO transition temperature, and then held at such temperature isothermally. During this process, polar diffraction patterns were obtained in regular time-steps. Such patterns were integrated along the polar angle, yielding the typical 1D diffraction spectra as a function of Bragg angle. Next, the [111] integrated intensity, I_{111}, was obtained as the area below the [111] diffraction peak, fitted using a Pseudo-Voigt profile. Finally, the change in degree of order between the initial SHT state and the stable equilibrium degree of order at the different annealing temperatures was calculated as the relative change of the square root of [111] integrated intensity, which should have a linear relationship with the volume fraction of $L2_1$ phase [[37], [38], [39], [40]].

3. Experimental results and prediction of the Curie temperature

3.1. Composition and thermal history dependence of Curie temperature

The evolution of T_C as a function of composition and annealing time at different secondary heat treatment (SecHT) temperatures below the ODO transition temperature is shown in Fig. 3. The data demonstrate a stronger dependence of T_C on the SecHT temperatures than on the duration of these treatments. In fact, the figure shows that most of the variation in T_C occurs within the first 15 min of the SecHTs. In general, T_C measured after SecHTs at 673 K and higher (up to 800 K) does not seem to be greatly affected by the duration of the heat treatment. On the other hand, in the case of the In13.55 alloy annealed at 573 K, 6 K difference in T_C can be seen between the samples annealed for 15 min vs those annealed for 3 days. The sluggish rate of change in the measured T_C as a function of treatment time at low temperatures is related to the rather sluggish kinetics of the ODO transition at these temperatures. An unintuitive feature of the evolution of T_C with the SecHTs is the case of the samples annealed at 873 K, which in all cases exhibit a T_C that is lower than the one measured when the samples were in the SHT condition. Below, it will be established that there is a monotonic dependence of T_C on the degree of η_{L21} order, which implies that under this particular heat treatment condition, the samples always have a lower degree of ηL21 order than those under the SHT condition.

The dependence of the T_C of the austenite on the SecHT temperature below the ODO transition temperature and alloy composition is presented in Fig. 4. Selected data for each SecHT temperature corresponds to the respective longest thermal treatment shown in Fig. 3. In addition, the T_C determined for the furnace cooled (FC) samples (refer to previous section for the details) has been included on the left side of the figure. The FC samples exhibit the highest T_C for all alloy compositions, as expected due to the slow cooling rates, making these samples the closest to their equilibrium state at low temperatures. In turn, the FC samples are expected to have the highest degree of $L2_1$ ordering among the samples studied here. It can be seen in the figure that there is a monotonic decrease of T_C with respect to the increasing SecHT temperature. This dependence becomes steeper when approaching the ODO transition temperature.

Notably, the SecHT temperature dependence of the T_C observed in Fig. 4 is similar to the temperature dependence of the $L2_1$ order parameter measured by Recarte et al. on a similar Ni-Mn-In MMSMA [40], where the authors observed a faster decrease in the ηL21, as the SecHT temperatures approached the ODO transition temperature. This temperature dependence of the order parameter below ODO temperature is the expected behavior of a second order transition [41]. However, previous works did not attempt to investigate how much time is required to achieve the thermal equilibrium degree of order at intermediate annealing temperatures. With this objective, in-situ transmission XRD experiments were performed on single crystal samples that were isothermally held at different annealing temperatures. Fig. 5 presents the Bragg angle dependence of the intensity diffracted by the [111], $L2_1$ order-dependent, and [200], order-independent, plane systems for four different samples. The first one, SHT, was measured at 423 K, and shows the initial state of the samples previous to the secondary heat treatments. The other three were measured at 680 K, 745 K and 790 K, respectively. Shown spectra were obtained shortly after the samples achieved thermal equilibrium degree of order: 15 min (10 min) for 680 K (745 and 790 K). Note that samples were held isothermally for about 1 h, but [111] integrated intensity remained constant after first 15 min of isothermal stage. This fact corroborates that the evolution of the overall degree of order on duration of the SecHT is the same as that observed for T_C. Fig. 5 also presents differences in peak position (angle of maximum) and peak broadening between samples. The former is the consequence of the thermal expansion, while the latter indicates the coarsening of the $L2_1$ ordering domains on increasing annealing temperature and time. More significantly, the inset in Fig. 5 presents a comparison between the square roots of the integrated intensity of the four samples, which is linearly dependent on the overall degree of order, ηL21. Similarly to what is observed for T_C in Fig. 3, the evolution of the integrated intensity indicates that the degree of order increases when the material is annealed at 680 and 745 K, while close to 773 K (790 K), the thermal equilibrium degree of order is similar to the one achieved during quenching from 1173 K (SHT state). It, thus, seems that there is a strong correlation between ηL21 and T_C, which has been shown previously for other MMSMAs [16,42]. The correlation in fact is so strong that T_C has recently been used by Neibecker et al. [34] to infer changes in the degree of order in similar alloy systems after different heat treatments. While, in principle, T_C could be affected by microstructural features other than the average degree of order, the relative invariance in the measured T_C with the heat treatment time (at temperatures of 673 K and above) suggests that in the present work, most of the change in T_C for different heat treatments is caused by the variations in the degree of $L2_1$ ordering.

3.2. Prediction of Curie temperature

To gain a better understanding of the underlying physics behind the connection between the T_C and η_{L21}, first-principles calculations were carried out. First, the magnetic exchange interaction parameters, determined using electronic structure calculations, were utilized to estimate the T_C using the Mean Field Approximation (MFA). These calculations were carried out using Spin-Polarized Relativistic Korringa-Kohn-Rostoker (SPRKKR) band structure code [43,44]. Single site Coherent Potential Approximation (CPA) was employed to account for the compositional disorder. The exchange-correlation potential was first modeled within the Generalized Gradient Approximation (GGA) of Perdew-Burke-Ernzerhof [45], and then it was utilized to determine the self-consistent potential by performing self-consistent calculations. The first step was to obtain the equilibrium lattice parameters for all compositions. To achieve this, the orbital momentum cut-off for the major component of the wave function was set as $l_{max}= 3$. Total energy converged within 0.01 mRy (Ry: Rydberg constant, 1 Ry = 13.606 eV). Secondly, the self-consistent potential was calculated to determine the equilibrium lattice parameters and Heisenberg magnetic exchange coupling parameters, $J_R^{\mu\nu}$, using the equation proposed by Liechtenstein et al. [46], where μ,ν correspond to different atomic species Ni, Co, Mn, or In, and R is the distance between μ and ν atoms.

For disordered systems, one or more sublattices, X, Y, or Z (specifically X_2YZ [47]), might be filled by several different atoms with different atomic concentrations. In such situation, it is useful to define the effective magnetic exchange parameters as function of atomic sites/sublattices. These effective exchange parameters between the sublattices P and Q, J_{eR}^{PQ}, with P, Q = X, Y or Z, were calculated by summing the weighted $J_R^{\mu\nu}$ [48]:

$$J_{eR}^{PQ} = \sum_{\mu\nu}^{Ni,Co,Mn,In} c_\mu(P) c_\nu(Q) J_0^{\mu\nu} \qquad (1)$$

where $c_{\mu/\nu}(P/Q)$ is the atomic concentration of element μ/ν in sublattice P/Q. In the particular case of a $Ni_{45}Co_5Mn_{36.5}In_{13.5}$ alloy presenting either B2 or $L2_1$ order structures, X sublattice is randomly occupied by Ni and Co atoms, $c_{Ni}(X) = 0.9$, $c_{Co}(X) = 0.1$, $c_{Mn,In}(X) = 0$; Y and Z contain only Mn or In atoms, $c_{Ni,Co}(Y,Z) = 0$, which can be distributed randomly in B2 phase, $c_{Mn}(Y,Z) = 0.73$, $c_{In}(Y,Z) = 0.27$, or ordered in $L2_1$ phase, $c_{Mn}(Y) = 1$, $c_{Mn}(Z) = 0.46$, $c_{In}(Y) = 0$, $c_{In}(Z) = 0.54$.

For a multi-lattice system, T_C can be obtained from the effective exchange parameter by solving the coupled equations (2), (3) [[49], [50], [51], [52]]:

$$\frac{3}{2}k_B T_c^{MFA} = \sum_Q J_e^{PQ} e^Q \quad (2)$$

$$J_e^{PQ} = \sum_{R \neq 0} J_{eR}^{PQ} \quad (3)$$

where k_B is the Boltzman constant, J_e^{PQ} is the total effective magnetic exchange parameter, and e^Q is the average z component of the unit (spin) vector E in the direction of the magnetic moment in the sublattice Q. We can restate Eqs. (2), (3)into an eigenvalue problem:

$$(\Theta - TI)E = 0, \quad \Theta_{PQ} = \frac{2J_e^{PQ}}{3k_B} \quad (4)$$

where I is the identity matrix, Θ is the matrix with elements Θ_{PQ}, and T are the eigenvalues. T_C of the system corresponds to the largest eigenvalue [[51], [52], [53], [54]].

The total effective magnetic exchange parameters calculated for $Ni_{45}Co_5Mn_{50-X}In_X$with X = 13.3, 13.5 or 13.7 MMSMAs, similar to the compositions experimentally studied here, as a function of the degree of $L2_1$ order, ηL21, are plotted in Fig. 6. Fig. 6a shows that the positive (ferromagnetic) magnetic exchange interactions between X and Y sites, J_e^{XY}, and between X and Z sites, J_e^{XZ}, are the main contributors to the ferromagnetism in the austenite phase. The third strongest ferromagnetic interaction occurs between Ni/Co and Ni/Co atoms in X sites, which is not shown in Fig. 6 since it is independent of degree of order, J_e^{XX}≈1.05 meV. Weaker positive contributions to the ferromagnetism occurs between Mn atoms in the same sublattice, either J_e^{YY} or J_e^{ZZ}, in Fig. 6b. Fig. 6c corroborates the fact that first nearest neighbor Mn atoms, those in different sublattices (Y and Z), interact antiferromagnetically, i.e. J_e^{YZ} is negative. However, the strength of these antiferromagnetic interactions is substantially lower than the ferromagnetic ones in austenite.

Calculations also show that when the degree of configurational order is increased to mimic the $L2_1$ state, J_e^{XY} and J_e^{YY} increase, J_e^{XZ} and J_e^{ZZ} decrease and J_e^{YZ} is practically unaffected. Such dependencies are consequence of the diffusion of Mn atoms from sublattice Z to Y, so the effective magnetic exchange parameters increase/decrease non-linearly depending on the amount of Mn atoms in Y and Z sites. Significantly, net increase of J_e^{XY} and J_e^{YY} contributions is larger than net decrease of J_e^{XZ} and J_e^{ZZ} ones, resulting in an enhancement of the ferromagnetic ordering with the increase of ηL21. Therefore, the calculations point out that in NiCoMnIn austenite, Mn-Mn antiferromagnetic interactions are overcome by ferromagnetic interactions, which become stronger as the configuration approaches $L2_1$-like ordering. This fact suggests a positive correlation between ηL21 and T_C, since enhancing the strength of the ferromagnetic interactions will increase T_C.

T_C was then calculated using the above magnetic exchange parameters by MFA for different degrees of order using Eq. (4). Fig. 7 shows T_C for three different compositions as a function of

η_{L21}. Curie temperature presents a monotonic non-linear increase with η_{L21}, which is related to the behavior of magnetic exchange parameters shown in Fig. 6. This relationship between T_C and η_{L21} is very similar to the measured experimental dependence of T_C on SecHT temperature, shown in Fig. 4, but with an opposite sign. Therefore, the present calculations support that T_C increases with η_{L21} and with decreasing In content, and confirm the inverse relationship between the degree of $L2_1$ order and the SecHT temperature.

Comparing Fig. 4, Fig. 7, it is obvious that there is a finite offset between the predicted and measured T_C as the predicted values are between 50 and 100 K higher than their experimental counterparts. There are several reasons for this discrepancy, including the absence of local ionic relaxations in the electronic structure calculations used. In fact, the CPA approach, by design, considers mixing in a given lattice site as a static superposition of electronic states and thus cannot account for the local differences in atomic environment arising from different site occupancies. Moreover, the predicted lattice parameters of the different NiCoMnIn alloys differ from those measured in the experiments — GGA calculations typically underestimate binding energies and overestimate interatomic separation. Magnetic exchange constants are very sensitive to interatomic distances and the mismatch between predicted and actual interatomic separations may be responsible for the observed discrepancy between the predicted and measured T_Cs. Furthermore, if one considers that T_C constitutes a measure of the energy scale of separation between a ferromagnetic and a paramagnetic state, a discrepancy of about 100 K roughly corresponds to an energy difference of about 10 meV/atom, well within the limit of the fidelity of first-principles calculations. Finally, we would like to point out that a similar offset was obtained by Şaşıoğlu et al. [54] when calculating T_C for Ni_2MnGa using magnetic exchange constants calculated with similar electronic structure approaches and within the same Mean Field Approximation.

4. Discussion of the results

As mentioned earlier, unraveling the relationship between T_C and η_{L21} is expected to provide a pathway to understand many of the significant effects recently observed in MMSMAs [19,28] subjected to arbitrary heat treatments. In fact, we propose that the observed dependence of T_C on the temperature and duration of the SecHTs is mostly caused by changes in the overall degree of $L2_1$ ordering in the microstructure, rather than on localized microstructural features, such as antiphase boundaries. If this is the case, we predict that T_C should be mostly determined by the kinetics of the ODO transition during different stages of the thermal history to which the samples are subjected to.

To establish a baseline behavior, we carried out a Solution Heat Treatment (SHT) at 1173 K for 24 h in order to ensure a state as close as possible to the B2 disordered state. From the experiments by Recarte et al. [40], it is known that for this alloy system, 1173 K is well above ODO transition temperature, and therefore, austenite should be in the B2 phase just before the samples are rapidly quenched. Further characterization of the samples, however, indicate that regardless of the as fast cooling rates as possible of the quenching procedure, a significant amount of $L2_1$ is already present in these samples, even before secondary heat treatments are carried out. For example, TEM dark field images of the same alloys considered in this study, using the [111]L21 superlattice reflections, show $L2_1$ domains of about 6–8 nm in a matrix of B2 phase [19,28].

In the present work, Fig. 3 shows that the SHT samples (quenched from 1173 K) present similar T_C values to the samples that were exposed to the SecHT at 773 K, and higher T_C values than the ones annealed at 873 K. Our experimental and computational results conclusively show that T_C is strongly associated with the degree of overall $L2_1$ ordering in the microstructure, and these observations point out that the ordering process cannot be suppressed by water quenching the samples. In other words, the kinetics of the ODO transition is fast enough to generate a significant amount of $L2_1$ states, even at the fast cooling rates resulting from water-quenching. Just a few seconds are thus sufficient to generate a non-negligible amount of $L2_1$ domains. This can be understood from the microscopic nature of the ordering process as the atomic exchange between Mn and In sublattices, necessary for the alloys to order/disorder, only involves a few atomic jumps over a diffusion distance corresponding to two nearest neighbors. It is thus to be expected that minute differences in the heat treatment and quenching procedure result in significant variability in the overall amount of $L2_1$ ordering and corresponding T_C. To reduce the impact of cooling rate on the results, all samples used for SecHTs for each composition were annealed within the same quartz ampoule and water quenched at the same time. This process guarantees that all samples used for SecHTs have similar initial ordered configurations. Despite the observed sensitivity of the state of SHT samples on quenching procedure, the dependence of the degree of $L2_1$ ordering on the quenching rate is expected to be not as significant for the samples under low temperature SecHTs since the ordering kinetics are expected to be sluggish when samples are quenched from low temperatures. This is verified in Fig. 4, which shows that for the samples heat treated at 573 K, the measured T_C is lower than that of the Furnace Cooled (FC) samples.

Since Tc changes are proportional to η_{L21} variations, Fig. 3 also describes (indirectly) the time evolution of the degree of order during different SecHT conditions. The figure shows how η_{L21} converges to an equilibrium value at longer heat treatment times. The figure also displays that for most heat treatment conditions above 673 K, the variation in T_C (and order parameter) takes place within the first 15 min of the heat treatment. These trends of the degree of order were corroborated using in-situ high-energy XRD experiments, Fig. 5, where the integrated intensity of the [111] diffraction peak is the order parameter-dependent property tracking the change in $B2/L2_1$ order. Another interesting trend is the observed variation of T_C with time for the samples annealed at 873 K. In this case, T_C is lower than that of the SHT samples, implying that the latter has a higher degree of $L2_1$ ordering. This can be reconciled as follows: (1) when quenching from SHT temperature, the ODO kinetics is fast enough to achieve a significant degree of order before atomic motion is ‘frozen in’; (2) the temperature corresponding to this ‘frozen-in’ state is lower than 873 K, since the SHT + WQ state has a higher η_{L21} than the SecHT-873 K sample. A similar behavior was also observed in Ref. [16], where a highly-ordered NiMnIn sample was heated from room temperature to 1000 K. The degree of $L2_1$ ordering parameter decreases from about

600 K to the ODO point following a power law, which is typical of these second order order-disorder transitions [37].

The fact that the degree of $L2_1$ ordering of the SHT samples, quenched from above the ODO temperature, can be higher than the one of samples annealed below the ODO point is apparently in conflict with the tendency shown in Fig. 4 — which only shows data for the SecHTs below the ODO temperature— but it is in agreement with previous works showing the HT temperature dependence of T_C above the ODO point [16,18,28]. In Ref. [16], Sánchez-Alarcos et al. showed that the quenching temperature dependence of T_C presents a minimum for NiMnGa alloys, which was shown to be about 20 K above the ODO transition temperature. The authors attributed this minimum to a non-monotonic relationship of the degree of $L2_1$ordering on quenching temperature. This can be explained by taking the role of thermal vacancies into consideration that above the ODO temperature, the samples may have the same degree of (dis)order but they definitely have very different concentrations of thermal vacancies. Since the ODO transition is mediated via (short-range) vacancy exchange, samples quenched from higher temperatures (above the ODO) may end-up having a higher degree of order because the ODO kinetics are accelerated through a higher initial concentration of vacancies, relative to the samples heat treated at lower temperatures (but still above the ODO).

After examination of the dependence of T_C on the SecHT temperature and duration, one can conclude that final degree of order presented by the material can be separated into two contributions: i) the degree of order present in the material previous to the cooling process, whose equilibrium value decreases with increasing the annealing temperature until it disappears above the ODO, and ii) ordering produced during cooling, which, with high enough cooling rate, increases with HT temperature due to the higher as-quenched vacancy concentrations and the resulting faster ordering kinetics due to enhanced atomic diffusion. The different dependence of these two contributions on the HT temperature is what generates the non-monotonous relationship between ηL21 and the HT temperature. It is expected that the same competition between the initial ordering state and the non-trivial dependence of ordering kinetics on heat treatment conditions and cooling rates is also the origin for the non-monotonous dependence of MT temperatures on HT temperature in different magnetic shape memory alloys, such as NiMnGa [16], NiCoMnIn [28] and NiFeGa [42].

In addition, the fact that ordering kinetics is fast has crucial repercussions on the interpretation of the recent results showing a non-monotonous annealing time dependence of MT temperatures in NiCoMnIn [28]. First, the variation of the total degree of $L2_1$ order only plays a significant role for short SecHTs by increasing the ferromagnetic ordering of austenite and decreasing M_S rapidly; and second, since T_C variations are small during long SecHTs, notable changes on M_S occurring during the same HTs should have a microstructural origin different than changes in the overall degree of $L2_1$ ordering in the microstructure of these systems.

Lastly, it is noted that the compositions for the present work were chosen within a range for which MT is very sensitive to compositional changes, i.e. X = 13.3 to 13.7 [15]. Within this compositional range, it is easy to obtain different degrees of MT arrest, which can lead to the strain glass transition, via simple heat treatments [19]. All figures here point out that the Curie temperature decreases on increasing In content. This effect is related with a weakening of ferromagnetic interaction between Ni sites and Mn sites, Fig. 4a, caused by the decrease of Mn content.

5. Summary and conclusions

In summary, the Curie temperature of austenite exhibits a monotonic dependence on the degree of $L2_1$ ordering. This relationship was verified via ab initiocalculations using the mean field approximation. The relationship between T_C and η_{L21} has been used to qualitatively estimate the evolution of the degree of order with secondary heat treatments performed below the ODO transition temperature. The results have shown that the ordering kinetics is fast, the total degree of order depends mostly on the secondary heat treatment temperature and cooling rate for long enough treatments, and maximum achievable ordering is limited by the low thermal energy available to atomic diffusion at low temperatures. Finally, small changes in composition have a strong impact on the MT temperatures and a significant but smaller effect on the ferromagnetic transition.

Acknowledgements

This work is supported by National Science Foundation (NSF), Division of Materials Research, Metals and Metallic Nanostructures Program, under the Grant no. DMR-1508634. DS and TD thank Dr. Ruben Santamarta for discussions on the effect of vacancy concentration on ordering and Dr. Claudio Schön for discussions regarding the first and second order transformations in these systems. This research used resources of the Advanced Photon Source, a U.S. Department of Energy (DOE) Office of Science User Facility operated for the DOE Office of Science by Argonne National Laboratory under Contract No. DE-AC02-06CH11357.

References

[1] V.A. Chernenko, C. Seguí, E. Cesari, J. Pons, V.V. Kokorin, Sequence of martensitic transformations in Ni-Mn-Ga alloys, Phys. Rev. B, 57 (1998), pp. 2659-2662.

[2] Y. Sutou, Y. Imano, N. Koeda, T. Omori, R. Kainuma, K. Ishida, K. Oikawa, Magnetic and martensitic transformations of NiMnX(X=In,Sn,Sb) ferromagnetic shape memory alloys, Appl. Phys. Lett., 85 (2004), pp. 4358-4360.

[3] M.A. Marioni, R.C. O'Handley, S.M. Allen, S.R. Hall, D.I. Paul, M.L. Richard, J. Feuchtwanger, B.W. Peterson, J.M. Chambers, R. Techapiesancharoenkij, The ferromagnetic shape-memory effect in Ni–Mn–Ga, J. Magn. Magn Mater., 290–291 (2005), pp. 35-41.

[4] R. Kainuma, Y. Imano, W. Ito, Y. Sutou, H. Morito, S. Okamoto, O. Kitakami, K. Oikawa, A. Fujita, T. Kanomata, K. Ishida, Magnetic-field-induced shape recovery by reverse phase transformation, Nature, 439 (2006), pp. 957-960.

[5] K. Ullakko, J.K. Huang, C. Kantner, R.C. O'Handley, V.V. Kokorin, Large magnetic-field-induced strains in Ni2MnGa single crystals, Phys. Lett., 69 (1996), pp. 1966-1968.

[6] I. Karaman, H.E. Karaca, B. Basaran, D.C. Lagoudas, Y.I. Chumlyakov, H.J. Maier, Stress-assisted reversible magnetic field-induced phase transformation in Ni2MnGa magnetic shape memory alloys, Scripta Mater., 55 (2006), pp. 403-406.

[7] R. Tickle, R.D. James, Magnetic and magnetomechanical properties of Ni2MnGa, J. Magn. Magn Mater., 195 (1999), pp. 627-638.

[8] E. Brück, Developments in magnetocaloric refrigeration, J. Phys. D Appl. Phys., 38 (2005), pp. R381-R391.

[9] T. Krenke, E. Duman, M. Acet, E.F. Wassermann, X. Moya, L. Mañosa, A. Planes, E.Suard, B. Ouladdiaf, Magnetic superelasticity and inverse magnetocaloric effect in Ni-Mn-In, Phys. Rev. B, 75 (2007), p. 104414.

[10] J.M. Barandiarán, V.A. Chernenko, P. Lázpita, J. Gutiérrez, J. Feuchtwanger, Effect of martensitic transformation and magnetic field on transport properties of Ni-Mn-Ga and Ni-Fe-Ga Heusler alloys, Phys. Rev. B, 80 (2009), p. 104404.

[11] N.M. Bruno, C. Yegin, I. Karaman, J.-H. Chen, J.H. Ross, J. Liu, Jianguo Li, The effect of heat treatments on Ni43Mn42Co4Sn11 meta-magnetic shape memory alloys for magnetic refrigeration, Acta Mater., 74 (2014), pp. 66-84.

[12] J.-H. Chen, N.M. Bruno, I. Karaman, Y. Huang, J. Li, J.H. Ross Jr., Direct measure of giant magnetocaloric entropy contributions in Ni–Mn–In, Acta Mater., 105 (2016), pp. 176-181.

[13] B.M. Wang, L. Wang, Y. Liu, B.C. Zhao, Y. Zhao, Y. Yang, H. Zhang, Strong thermal-history-dependent magnetoresistance behavior in Ni49.5Mn34.5In16, J. Appl. Phys., 106 (2009) 063909.

[14] J. Pons, V.A. Chernenko, R. Santamarta, E. Cesari, Crystal structure of martensitic phases in Ni–Mn–Ga shape memory alloys, Acta Mater., 48 (2000), pp. 3027-3038.

[15] W. Ito, Y. Imano, R. Kainuma, Y. Sutou, K. Oikawa, K. Ishida, Martensitic and magnetic transformation behaviors in Heusler-Type NiMnIn and NiCoMnIn metamagnetic shape memory alloys, Metall. Mater. Trans., 38 (2007), pp. 759-766.

[16] V. Sánchez-Alarcos, V. Recarte, J.I. Pérez-Landazábal, G.J. Cuello, Correlation between atomic order and the characteristics of the structural and magnetic transformations in Ni–Mn–Ga shape memory alloys, Acta Mater., 55 (2007), pp. 3883-3889.

[17] W. Ito, M. Nagasako, R.Y. Umetsu, R. Kainuma, T. Kanomata, K. Ishida, Atomic ordering and magnetic properties in the Ni45Co5Mn36.7In13.3 metamagnetic shape memory alloy, Appl. Phys. Lett., 93 (2008), p. 232503.

[18] V. Sánchez-Alarcos, V. Recarte, J.I. Pérez-Landazábal, E. Cesari, J.A. Rodríguez-Velamazán, Long-range atomic order and entropy change at the martensitic transformation in a Ni-Mn-in-Co metamagnetic shape memory alloy, Entropy, 16 (2014), pp. 2756-2767.

[19] J.A. Monroe, J.E. Raymond, X. Xu, M. Nagasako, R. Kainuma, Y.I. Chumlyakov, R.Arroyave, I. Karaman, Multiple ferroic glasses via ordering, Acta Mater., 101 (2015), pp. 107-115.

[20] R.Y. Umetsu, W. Ito, K. Ito, K. Koyama, A. Fujita, K. Oikawa, T. Kanomata, R. Kainuma, K. Ishida, Anomaly in entropy change between parent and martensite phases in the Ni50Mn34In16 Heusler alloy, Scripta Mater., 60 (2009), pp. 25-28.

[21] E. Cesari, D. Salas, S. Kustov, Entropy changes in ferromagnetic shape memory alloys, Mater. Sci. Forum, 684 (2011), pp. 49-60.

[22] A.M. Pérez-Sierra, N.M. Bruno, J. Pons, E. Cesari, I. Karaman, Atomic order and martensitic transformation entropy change in Ni–Co–Mn–In metamagnetic shape memory alloys, Scripta Mater., 110 (2016), pp. 61-64.

[23] S. Kustov, M.L. Corró, J. Pons, E. Cesari, Entropy change and effect of magnetic field on martensitic transformation in a metamagnetic Ni–Co–Mn–In shape memory alloy ,Appl. Phys. Lett., 94 (2009), p. 191901.

[24] W. Ito, K. Ito, R.Y. Umetsu, R. Kainuma, Kinetic arrest of martensitic transformation in the NiCoMnIn metamagnetic shape memory alloy, Appl. Phys. Lett., 92 (2008) 021908.

[25] H.E. Karaca, I. Karaman, B. Basaran, Y. Ren, Y.I. Chumlyakov, H.J. Maier, Magnetic field-induced phase transformation in NiMnCoIn magnetic shape-memory alloys-A new actuation mechanism with large work output, Adv. Funct. Mater., 19 (2009), pp. 983-998.

[26] Y. Wang, C. Huang, J. Gao, S. Yang, X. Ding, X. Song, X. Ren, Evidence for ferromagnetic strain glass in Ni-Co-Mn-Ga Heusler alloy system, Appl. Phys. Lett., 101 (2012), p. 101913.

[27] X. Ren, Strain glass and ferroic glass – unusual properties from glassy nano-domains, Phys. Status Solidi B, 251 (2014), pp. 1982-1992.

[28] N.M. Bruno, D. Salas, S. Wang, I.V. Roshchin, R. Santamarta, R. Arroyave, T. Duong, Y.I.Chumlyakov, I. Karaman, On the microstructural origins of martensitic transformation arrest in a NiCoMnIn magnetic shape memory alloy, Acta Mater., 142 (2018), pp. 95-106.

[29] P.J. Stonaha, I. Karaman, R. Arroyave, D. Salas, N.M. Bruno, Y. Wang, M.F. Chisholm, S.Chi, D.L. Abernathy, Y.I. Chumlyakov, M. E Manley, Glassy phonon Heralds a strain glass state in a shape memory alloy, Phys. Rev. Lett., 120 (2018), p. 245701.

[30] C. Seguí, E. Cesari, Contributions to the transformation entropy change and influencing factors in metamagnetic Ni-Co-Mn-Ga shape memory alloys, Entropy, 16 (2014), pp. 5560-5574.

[31] V.D. Buchelnikov, P. Entel, S.V. Taskaev, V.V. Sokolovskiy, A. Hucht, M. Ogura, H. Akai, M.E. Gruner, S.K. Nayak, Monte Carlo study of the influence of antiferromagnetic exchange interactions on the phase transitions of ferromagnetic Ni-Mn-X alloys (X=In,Sn,Sb), Phys. Rev. B, 78 (2008), p. 184427.

[32] T. Miyamoto, M. Nagasako, R. Kainuma, Phase equilibria in the Ni–Mn–In alloy system, J. Alloy. Comp., 459 (2013), pp. 57-63.

[33] K. Oikawa, T. Ota, T. Ohmori, Y. Tanaka, H. Morito, A. Fujita, R. Kainuma, K.Fukamichi, K. Ishida, Magnetic and martensitic phase transitions in ferromagnetic Ni–Ga–Fe shape memory alloys, Appl. Phys. Lett., 81 (2002), pp. 5201-5203.

[34] P. Neibecker, M. Leitner, G. Benka, W. Petry, Increasing the achievable state of order in Ni-based Heusler alloys via quenched-in vacancies, Appl. Phys. Lett., 105 (2014), p. 261904.

[35] S. Kustov, I. Golovin, M.L. Corró, E. Cesari, Isothermal martensitic transformation in metamagnetic shape memory alloys, J. Appl. Phys., 107 (2010) 053525.

[36] V.K. Pecharsky, K.A. Gschneidner Jr., Giant magnetocaloric effect in Gd5(Si2Ge2), Phys. Rev. Lett., 78 (1997), pp. 4494-4497.

[37] A. Planes, Ll Mañosa, E. Vives, J. Rodriguez-Carvajal, M. Morin, G. Guénin, J.L.Macqueron, Neutron diffraction study of long-range atomic order in Cu-Zn-Al shape memory alloys, J. Phys. Condens. Matter, 4 (1992), pp. 553-559.

[38] T. Krenke, M. Acet, E.F. Wassermann, X. Moya, L. Mañosa, A. Planes, Martensitic transitions and the nature of ferromagnetism in the austenitic and martensitic states of Ni-Mn-Sn alloys, Phys. Rev. B, 72 (2005) 014412.

[39] V. Sánchez-Alarcos, J.I. Pérez-Landazábal, V. Recarte, I. Lucia, J. Vélez, J.A. Rodríguez-Velamazán, Effect of high-temperature quenching on the magnetostructural transformations and the long-range atomic order of Ni–Mn–Sn and Ni–Mn–Sb metamagnetic shape memory alloys, Acta Mater., 61 (2013), pp. 4676-4682.

[40] V. Recarte, J.I. Pérez-Landazábal, V. Sánchez-Alarcos, J.A. Rodríguez-Velamazán, Dependence of the martensitic transformation and magnetic transition on the atomic order in Ni–Mn–In metamagnetic shape memory alloys, Acta Mater., 60 (2012), pp. 1937-1945.

[41] L.D. Landau, E.M. Lifshitz, Stadistical Physics (third ed.), Pergamon Press Inc., New York (1963).

[42] R. Santamarta, E. Cesari, J. Font, J. Muntasell, J. Pons, J. Dutkiewicz, Effect of atomic order on the martensitic transformation of Ni–Fe–Ga alloys, Scripta Mater., 54 (2006), pp. 1985-1989.

[43] H. Ebert, D. Ködderitzsch, J. Minár, Calculating condensed matter properties using the KKR-Green's function method—recent developments and applications, Rep. Prog. Phys, 74 (2011) 096501.

[44] H. Ebert, The Munich SPR-KKR Package, Version 6.3 http://ebert.cup.uni-muenchen.de/SPRKKR.

[45] M. Ernzerhof, G.E. Scuseria, Assessment of the perdew–Burke–Ernzerhof exchange-correlation functional, J. Chem. Phys., 110 (1999), pp. 5029-5036.

[46] A.I. Liechtenstein, M.I. Katsnelson, V.A. Gubanov, Exchange interactions and spin-wave stiffness in ferromagnetic metals, J. Phys. F Met. Phys., 14 (1984), pp. L125-L128.

[47] T. Graf, C. Felser, S.S.P. Parkin, Simple rules for the understanding of Heusler compounds,Prog. Solid State Chem., 39 (2011), pp. 1-50.

[48] A.I. Liechtenstein, M.I. Katsnelson, V.P. Antropov, V.A. Gubanov, Local spin density functional approach to the theory of exchange interactions in ferromagnetic metals and alloys, J. Magn. Magn Mater., 67 (1987), pp. 65-74.

[49] N. Singh, E. Dogan, I. Karaman, R. Arróyave, Effect of configurational order on the magnetic characteristics of Co-Ni-Ga ferromagnetic shape memory alloys, Phys. Rev. B, 84 (2011), p. 184201.

[50] N. Singh, R. Arróyave, Magnetocaloric effects in Ni-Mn-Ga-Fe alloys using Monte Carlo simulations, J. Appl. Phys., 113 (2013), p. 183904.

[51] E. Şaşıoğlu, L.M. Sandratskii, P. Bruno, First-principles calculation of the intersublattice exchange interactions and Curie temperatures of the full Heusler alloys Ni2MnX (X = Ga, In, Sn, Sb), Phys. Rev. B, 70 (2004), p. 24427.

[52] M. Meinert, J.-M. Schmalhorst, G. Reiss, Ab initio prediction of ferrimagnetism, exchange interactions and Curie temperatures in Mn2TiZ Heusler compounds, J. Phys. Condens. Matter, 23 (2011) 036001.

[53] P.W. Anderson, Theory of magnetic exchange interactions: exchange in insulators and semiconductors, Solid State Phys., 14 (1963), pp. 99-214.

[54] E. Şaşıoğlu, L.M. Sandratskii, P. Bruno, I. Galanakis, Exchange interactions and temperature dependence of magnetization in half-metallic Heusler alloys, Phys. Rev. B, 72 (2005), p. 184415.

Table 1. Measured compositions of the alloys fabricated in the present work, using Wavelength Dispersive Spectroscopy.

Composition (at.%)	**Ni**	**Co**	**Mn**	**In**
$NiCoMnIn_{13.55}$ (In13.55)	44.97 ± 0.10	5.05 ± 0.07	36.42 ± 0.12	13.55 ± 0.05
$NiCoMnIn_{13.71}$ (In13.71)	45.16 ± 0.06	5.04 ± 0.09	36.09 ± 0.10	13.71 ± 0.06
$NiCoMnIn_{13.92}$ (In13.92)	44.97 ± 0.14	5.01 ± 0.09	36.09 ± 0.17	13.92 ± 0.04

Figure Caption

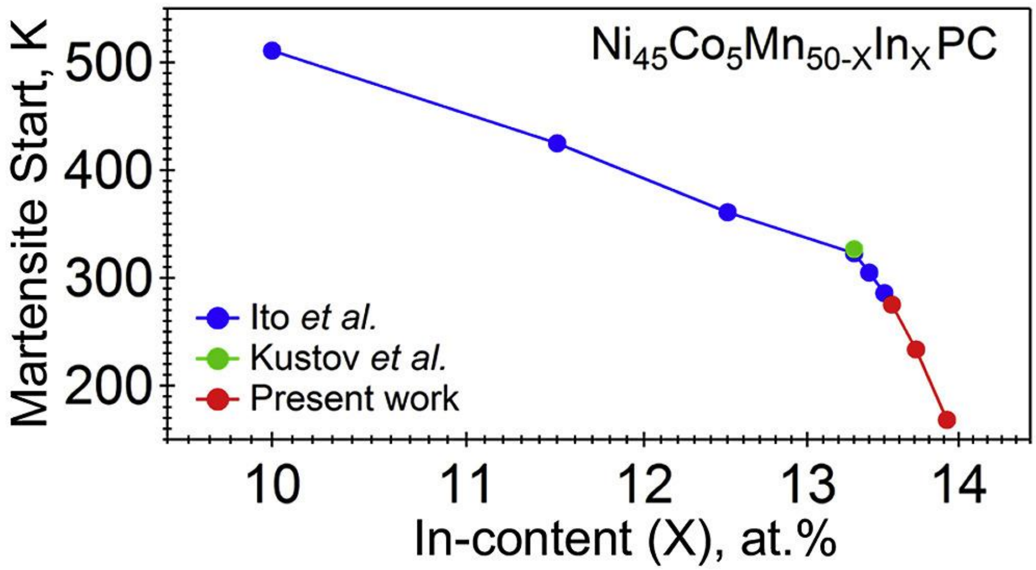

Fig. 1. In-content dependence of Martensite Start temperature, M_S, for solution heat treated samples of polycrystalline $Ni_{45}Co_5Mn_{50-X}In_X$ at.%. Plot compares data obtained for present work material (in red) with published data in the literature (in blue [15] and green [35]).

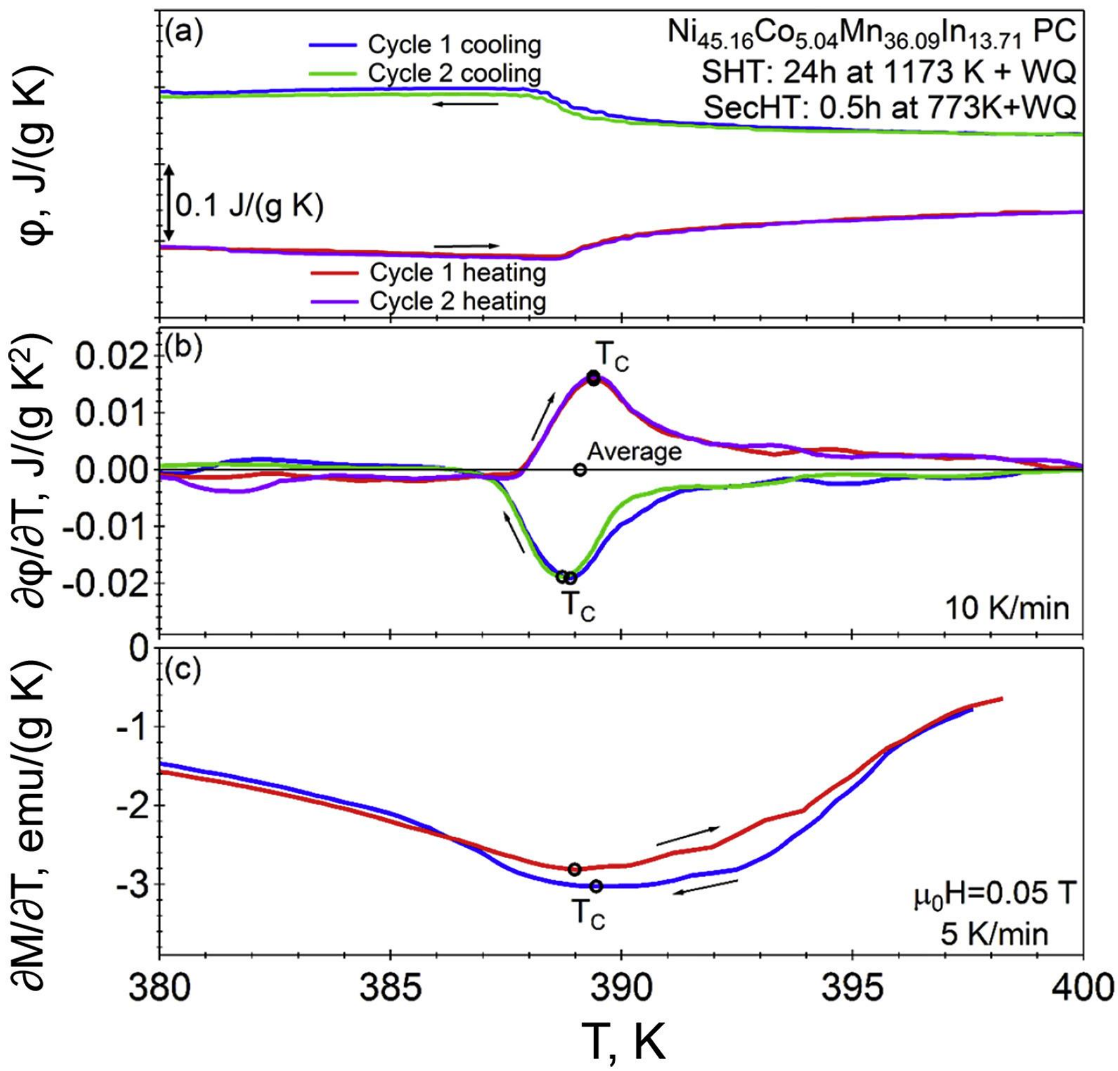

Fig. 2. Comparison between the temperature dependences of (a) the calorimetric response, φ, normalized by sample mass and temperature rate, and (b) its temperature derivative, $\partial\varphi/\partial T$, during two thermal cycles and (c) the temperature derivative of the total magnetization, $\partial M/\partial T$, during a single cooling/heating cycle under a constant magnetic field of 0.05 T, both for the same sample of polycrystalline (PC) $NiCoMnIn_{13.71}$Meta-Magnetic Shape Memory Alloy (MMSMA), solutionized at 1173 K for 24 h (WQ) and secondary annealed at 773 K for 0.5 h followed by water quenching. Arrows indicate the direction of cooling/heating of the temperature cycles. Open circles in (b) indicate the peak temperatures from which the Curie temperature was calculated as an average of the four curves (displayed in the middle). This value is compared with Curie temperature measured from thermo-magnetization curves in (c).

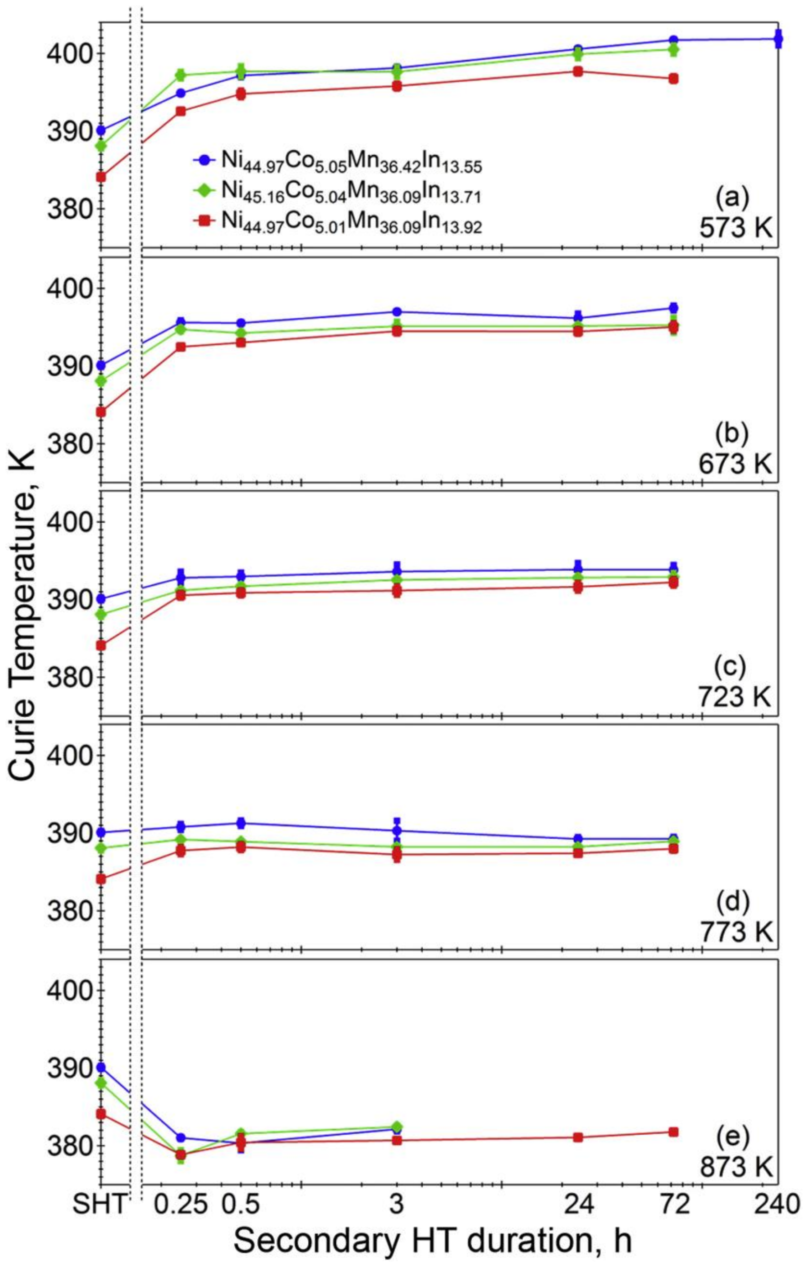

Fig. 3. The evolution of the Curie temperature (T_C) of the austenite in polycrystalline(PC) $NiCoMnIn_x$ MetaMagnetic Shape Memory Alloys (MMSMAs) with X = 13.55 (blue circles), X = 13.71 (green diamonds) and X = 13.92 (red squares), as a function of secondary heat treatment (Secondary HT) temperature and time. T_C was determined using calorimetric measurements. Secondary Heat Treatments: (a) 573 K, (b) 673 K, (c) 723 K, (d) 773 K and (e) 873 K. The initial state of the samples before Secondary HT was established using solution heat treatment at 1173 K followed by water quenching. Error bars represent the standard deviations after averaging the measured Curie temperatures for the different cooling and heating runs, see Fig. 1.

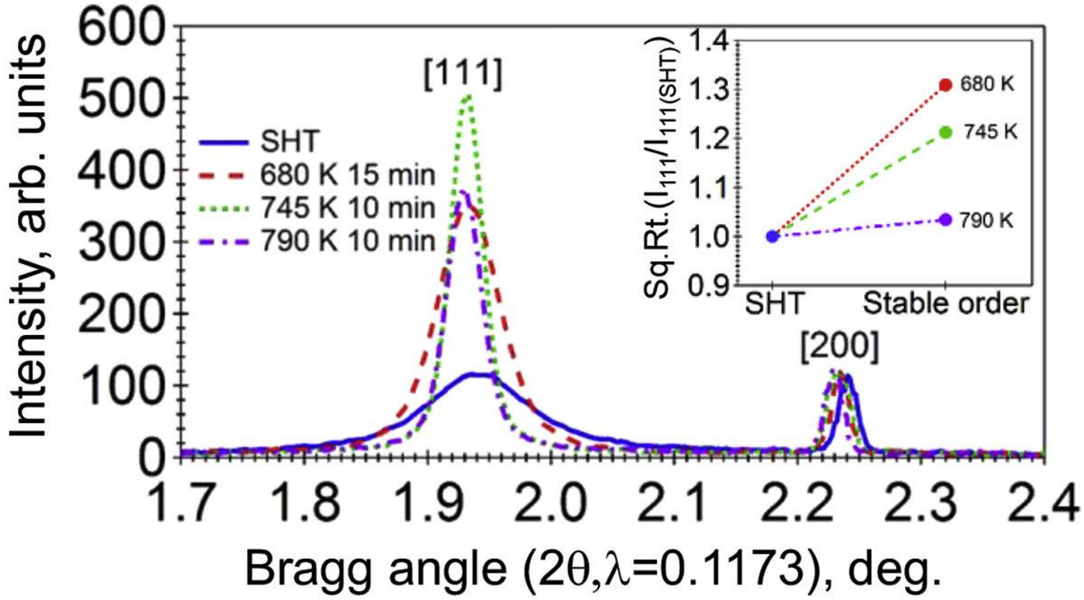

Fig. 5. Transmission X-ray diffraction spectra covering [111] and [200] peaks for four different SHT single crystalline $Ni_{45}Co_5Mn_{36.6}In_{13.4}$ samples, measured either at room temperature, SHT (solid blue), or at different temperatures after thermal equilibrium degree of order have been achieved, 680 K (long dashed red), 745 K (short dashed green) and 790 K (dashed with points purple). Time required to achieve stable order was 15 min for 680 K and <10 min for higher annealing temperatures. Inset shows the relative change of the square root of the integrated intensity of the [111] peak, I_{111}, between initial and annealed states, closely related with $L2_1$ degree of order, η_{L21}.

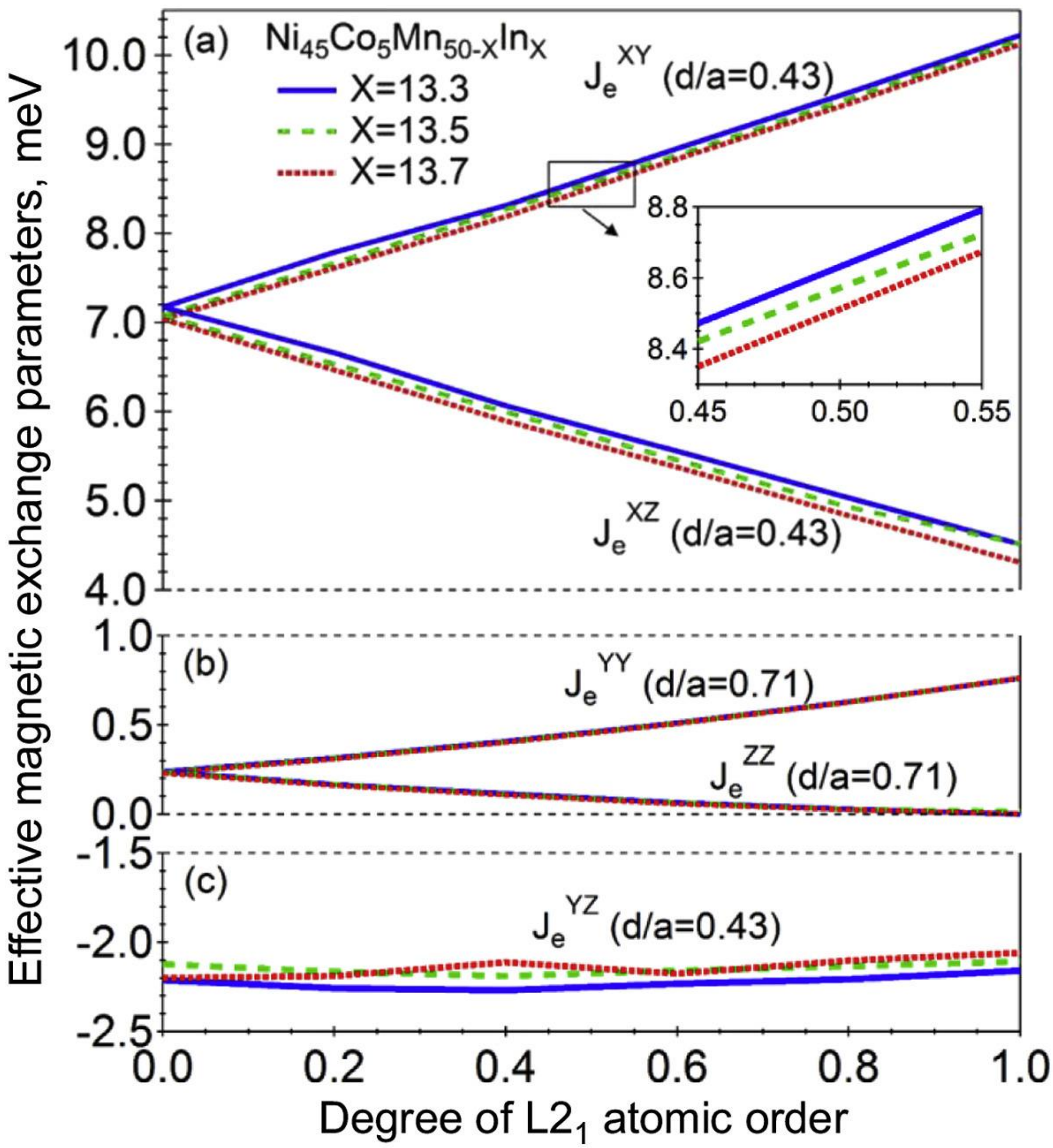

Fig. 6. Calculated total effective magnetic exchange parameters, a) J_e^{XY} and J_e^{XZ}, b) $J_e^{YY}$and J_e^{ZZ}, and c) J_e^{YZ}, as function of the degree of L2$_1$ ordering, ηL21, in the austenitephase of $Ni_{45}Co_5Mn_{50-x}In_x$ MMSMAs with X = 13.3 (solid black line), X = 13.5 (dashed blue line) and X = 13.7 (fine dashed green line). Inset in (a) is a zoomed in version of the plot showing the dependence of J_e^{XY} on In content more clearly. d/a is the ratio of the distance between the P and Q sites, d, and the lattice parameter, a.

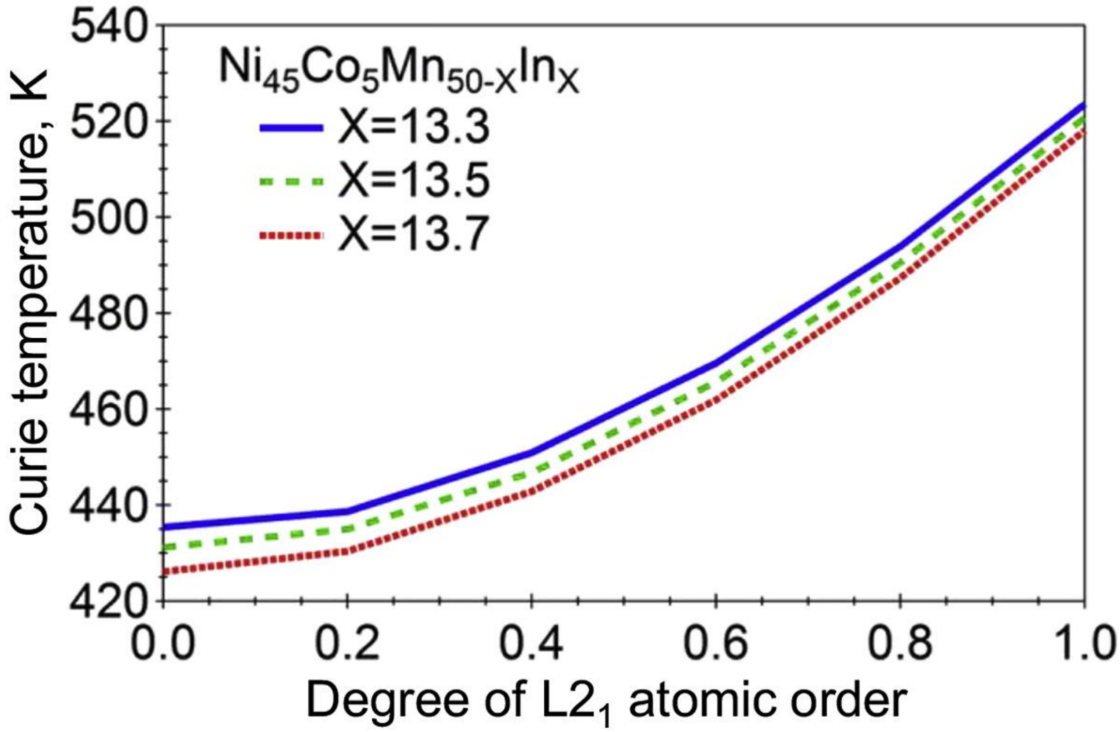

Fig. 7. Predicted Curie temperature, T_C of the austenite phase as a function of the degree of $L2_1$ order in $Ni_{45}Co_5Mn_{50-x}In_x$ MMSMAs, where X = 13.3 (solid black), 13.5 (dashed blue) and 13.7 (fine dashed green). (For interpretation of the references to colour in this figure legend, the reader is referred to the Web version of this article.)

Graphical abstract